 

***LASERS***

https://doi.org/10.1070/QEL17594

# Formation of a waveguide in a LiF crystal by a mid-IR light bullet

A.V. Kuznetsov, A.E. Dormidonov, V.O. Kompanets, S.V. Chekalin, V.P. Kandidov

***Abstract.*** **We report experimental and numerical investigation of the dynamics of the onset of micromodifications in a LiF crystal upon filamentation of femtosecond mid-IR radiation under conditions of anomalous group velocity dispersion with an increase in the number of acting pulses. It is found that the length of the induced waveguide increases with an increase in the number of acting pulses both in the direction of radiation propagation and in the opposite direction, reaching about 5 mm with an exposure of several thousand pulses. A model is proposed for the waveguide structure formation upon accumulation of changes in the LiF refractive index, caused by the formation of colour centres under conditions of saturation of their concentration. It is shown that the refractive index transverse distribution in the structure has a table-like shape with a diameter of more than 4 μm, which leads to the localisation of radiation reflected from the boundaries of the waveguide.**

***Keywords:*** *filamentation, femtosecond pulses, light bullets, micro waveguides, colour centres, LiF.*

## 1. Introduction

High power density and short duration of femtosecond pulses make it possible to implement photoinduced micromodification of optical materials without thermal destruction. For the first time, the possibility of recording an optical waveguide in the bulk of optical materials with near-IR radiation was demonstrated in Refs [1, 2]. The micromodification of the medium in tightly focused beams makes it possible to form planar and three-dimensional elements of integrated optics, such as splitters [3] and fibre Bragg gratings [4, 5]. During filamentation of femtosecond radiation due to the dynamic balance of Kerr self-focusing and defocusing in a laser plasma, a high intensity is maintained at a distance significantly exceeding the Rayleigh length [6, 7]. In this regime, the micromodification channel is formed in the filament and, with increasing exposure time, lengthens along the direction of radiation propagation [8]. Using filament-induced micromodifications, waveguide couplers [9–11], hexagonal arrays of coupled waveguides [12], diffraction gratings [13], focusing transparencies [14], and other elements of micro-optics [15] were obtained.

A significant part of the research on micromodification of materials was carried out for quartz, and the increase in its refractive index upon exposure to intense radiation is explained using various models based on the processes of rapid cooling of molten glass in the focal region [16], as well as the relaxation of free carriers arising in laser plasma [17]. The influence of the accumulation of refractive index micromodification in fused silica on multiple filamentation of femtosecond radiation was studied in Ref. [18].

Alkali metal fluorides are promising materials for fabricating microoptical elements, among which the LiF crystal, which has the widest transparency region and band gap (about 14 eV) among all transparent dielectrics [19], occupies a special place. In addition, LiF is characterised by high thermal and optical stability, low hygroscopicity, and properties that are convenient for mechanical processing.

Filamentation of femtosecond laser pulses in LiF leads to the formation of various types of the electronic subsystem excitations, such as anionic electron–hole pairs and excitons, the decay of which leads to the formation of the observed long-lived colour centres (CCs) [20–23]. The energy of electron–hole pairs and excitons in LiF is released through three physical channels: in the form of heat, luminescence, and the formation of primary radiation defects, the so-called Frenkel pairs. Some of them, through a sequence of reactions [23], transform into more complex crystal lattice defects, aggregate colour centres, including $F_2$ and $F_2^+$ centres stably luminescent in the visible range.

The refractive index of coloured LiF differs from the initial refractive index of LiF by a certain value $\Delta n_c$, which depends on the wavelength and concentrations of different types of colour centres. The modification of the refractive index induced by multipulse action is capable of forming a waveguide in the bulk of the LiF crystal [24]. During filamentation of radiation pulses at 2600–3500 nm in LiF, which belong to the region of anomalous group velocity dispersion (AGVD), single-cycle high-intensity light bullets (LBs) are formed [25–27], along the path of which CCs are generated. With an increase in the number of acting pulses, the length of the waveguide induced in LiF increases, and the spectrum of the supercontinuum generated by the LB undergoes a qualitative transformation due to the appearance of the guided propagation regime [28].

In this work, the dynamics of the formation of an extended waveguide in a LiF crystal with an increase in the number of acting femtosecond pulses in the mid-IR range under AGVD

**A.V. Kuznetsov** Irkutsk Branch of the Institute of Laser Physics, Siberian Branch, Russian Academy of Sciences, ul. Lermontova 130a, 664033 Irkutsk, Russia; e-mail: a.v.kuznetsov@bk.ru;
**A.E. Dormidonov, V.O. Kompanets, S.V. Chekalin** Institute of Spectroscopy, Russian Academy of Sciences, ul. Fizicheskaya 5, 108840 Moscow, Troitsk, Russia; e-mail: chekalin@isan.troitsk.ru;
**V.P. Kandidov** Institute of Spectroscopy, Russian Academy of Sciences, ul. Fizicheskaya 5, 108840 Moscow, Troitsk, Russia; Faculty of Physics, Lomonosov Moscow State University, Vorob'evy Gory, 119991 Moscow, Russia; e-mail: kandidov@physics.msu.ru

Received 9 June 2021
*Kvantovaya Elektronika* **51** (8) 670–678 (2021)
Translated by V.L. Derbov

conditions is studied experimentally and numerically. A model is proposed for the formation of a waveguide upon a change in the refractive index in LiF caused by the formation of colour centres under conditions of saturation of their concentration and waveguide capture of radiation by a structure induced during filamentation of mid-IR femtosecond pulses and the formation of a LB.

## 2. Measurement technique and experimental results

The waveguides in the LiF crystal were recorded using a Tsunami femtosecond oscillator (Ti:sapphire laser) with a Millenia Vs cw solid-state pump laser, a Spitfire Pro regenerative amplifier pumped by an Empower 30 pulsed solid-state laser, and a TOPAS-C tunable parametric amplifier. We used radiation pulses at $\lambda = 3200$ nm with a FWHM duration of 100 fs and a beam radius of 4 mm at a low repetition rate (4 Hz) to exclude thermal effects. The pulse energy was measured with photo- and pyroelectric detectors calibrated against the PS-10 detector. Laser pulses were focused on the front face of the LiF sample with a thin $CaF_2$ lens having a focal length $F = 10$ cm, at which the beam diameter at the input face of the sample was 120–150 μm. To obtain the LB in the single filamentation regime, pulses with an energy of 25 μJ were used.

Waveguides formed by CCs in LiF were recorded upon a sequential increase in the number of acting pulses from one–two to 2500. The analysis of the resulting waveguides was carried out usingthe CC luminescent radiation excited by cw laser radiation at $\lambda = 450$ nm. Luminescence was recorded with a Nikon D800 digital camera with a Euromex Oxion 5 microscope. In this case, the scattered exciting radiation was cut off by a yellow-green light filter. The distance from the input face of the sample to the beginning of the waveguide was about 4 mm in the single-pulse exposure regime and decreased with an increase in the number of pulses.

Luminescent waveguides made of long-lived CCs recorded in LiF under the action of different numbers of femtosecond laser pulses with the above parameters are shown in Fig. 1.


**Figure 1.** Photographs of luminescent waveguides made of long-lived CCs recorded in LiF under the action of a different number of femtosecond laser pulses with $\lambda = 3200$ nm. CCs excited by a cw laser with a radiation wavelength of 450 nm make a contribution to the visible luminescence. Femtosecond pulses travel from left to right; numbers on the left are the number of pulses.

It is seen that with an increase in the number of pulses, the length of the induced waveguides increases both in the direction of radiation propagation (to the right) and in the opposite direction. In the direction of the pulse propagation, the length of the tracks increases significantly, reaching 5 mm with an exposure of several thousand pulses. An increase in the length indicates that CC structures transparent in the mid-IR range improve the conditions for the appearance and propagation of LBs rather than prevent their formation during the creation of a waveguide. The appearance of a single-cycle LB at the output of the induced waveguide, detected by the oscillations of the CC concentration in the observed track, were more frequent in the first tens of pulses and more rare with their subsequent increase. Under the action of 200 or more pulses, the CC concentration in the direction of pulse propagation changes nonmonotonically. This is apparently due to the delocalisation of the LB radiation at the waveguide exit and its repeated compression, which is clearly registered from the CC concentration oscillations characteristic of a single-cycle LB [25]. It should be noted that, in the induced waveguide, the LB is formed in a pulse, the peak power of which only slightly exceeds the critical self-focusing power. The elongation of the waveguide in the direction opposite to the propagation of radiation with an increase in the number of pulses is about 1 mm and occurs mainly with the accumulation of the modification caused by the first several tens of pulses. With an increase in their number, the displacement of the waveguide beginning slows down and reaches a stationary value after exposure to several thousand pulses (Fig. 2).

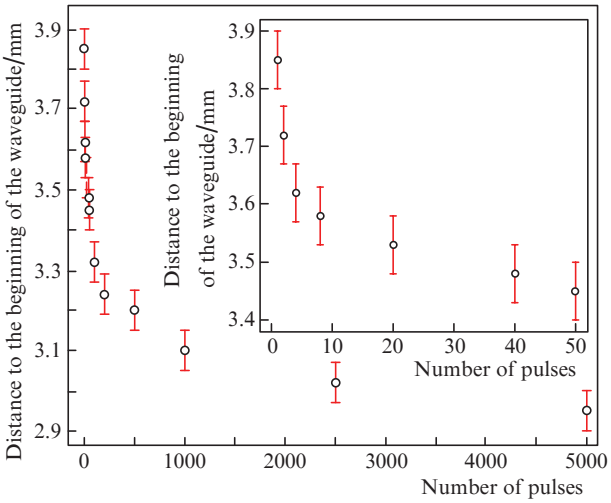


**Figure 2.** Displacement of the beginning of the waveguide towards the direction of pulse propagation in LiF with an increase in the number of acting radiation pulses at $\lambda = 3200$ nm.

## 3. Model of the change in the refractive index during the generation of colour centres in LiF

The numerical study is based on a model that describes, during femtosecond filamentation, changes in the LiF refractive index caused by the formation of colour centres under conditions of saturation of their concentration, waveguide capture of radiation by a structure induced by pulses, and the effect of fluctuations in their energy. The spatial distribution of stable CCs is described by the effective concentration $\rho_c$ of all types of CCs, which is accumulated pulse by pulse and reaches saturation $\rho_{c_{max}}$ at a sufficiently large number of pulses. The induced increment of the refractive index $\Delta n_c$ is proportional to the CC concentration:

$$\Delta n_c = \beta \rho_c, \qquad (1)$$

where $\beta$ is the proportionality coefficient. In the model, each pulse of the series, starting from the second pulse, propagates at a changed refractive index in a medium with colour centres, which are assumed to be completely formed from electron–hole pairs and excitons induced by previous pulses. In this case, subsequent laser pulses do not destroy the CC structure created by the previous ones.

In the general case, exposure to laser radiation leads to the formation of both excitons with a concentration $\rho_{ex}(\boldsymbol{r},t)$ and electron–hole pairs with a concentration $\rho_{eh}(\boldsymbol{r},t)$ equal to the concentration of free electrons $\rho_e(\boldsymbol{r},t)$ in the induced laser plasma. The kinetic equations describing the change in the concentrations of free electrons $\rho_e(\boldsymbol{r},t)$ and excitons $\rho_{ex}(\boldsymbol{r},t)$ in a light field with an amplitude $A(\boldsymbol{r},t)$ have the form:

$$\frac{\partial\rho_e(\boldsymbol{r},t)}{\partial t} = (1-\alpha) \times\left[W_E(|A|)\left(1-\frac{\rho_e(\boldsymbol{r},t)+\rho_{ex}(\boldsymbol{r},t)}{\rho_0}\right)+\nu_i\rho_e(\boldsymbol{r},t)\right], \quad (2a)$$

$$\frac{\partial\rho_{ex}(\boldsymbol{r},t)}{\partial t} = \alpha\left[W_{ex}(|A|)\left(1-\frac{\rho_e(\boldsymbol{r},t)+\rho_{ex}(\boldsymbol{r},t)}{\rho_0}\right)\right], \quad (2b)$$

where $\nu_i \approx 10^{15}$ s$^{-1}$ is the rate of inelastic collisions of electrons and ions of the crystal lattice, and $\rho_0 = 6.1\times10^{22}$ cm$^{-3}$ is the concentration of fluorine anions in LiF. The ionisation of lithium cations can be ignored, because it requires more energy and is therefore less likely. The field ionisation rate $W_E(|A|)$ is described by the Keldysh formula [29]. Equation (2a) does not take into account the recombination of electron–hole pairs. The function $W_{ex}(|A|)$ in (2b) is the rate of direct generation of excitons per unit volume. The exciton absorption energy is $U = 12.8$ eV, which is close to the band gap in LiF, which is estimated at 13.5 eV [30]. At the mid-IR wavelength, the direct exciton generation channel in LiF is a multiphoton process. Models of the direct exciton generation channel are currently unknown. At an exciton absorption energy close to the band gap, it can be assumed that the functions describing the exciton generation rate $W_{ex}(|A|)$ and the field ionisation rate $W_E(|A|)$ coincide. Equations (2a) and (2b) describe a decrease in the rate of field ionisation with the formation of electrons and the rate of direct generation of excitons with an increase in their total concentration due to a decrease in the number of unexcited anions in the crystal lattice. Parameter $\alpha$ in (2a) and (2b), which determines the relative contribution of the exciton and electron–hole channels of CC generation, takes values from zero to unity; $\alpha = 0$ and 1 correspond, respectively, to the formation of colour centres only through the electron–hole channel and through the exciton channel only.

The increment in the concentration of colour centres $\delta\rho_c(\boldsymbol{r})$, created by a single pulse, is proportional to the sum of the concentrations of electron–hole pairs $\delta\rho_{eh}(\boldsymbol{r})$ and excitons $\delta\rho_{ex}(\boldsymbol{r})$ accumulated during the pulse propagation, corresponding to two excitation channels of the electron subsystem, whose contributions can be considered equal:

$$\delta\rho_c = h(\delta\rho_{eh}+\delta\rho_{ex}), \quad (3)$$

where $h < 1$ is the coefficient of transformation of the concentrations of electron–hole pairs and excitons into an increment in the concentration of colour centres.

At saturation, the CC concentration $\rho_c^j(\boldsymbol{r})$ accumulated after the impact of the $j$th pulse is represented in the form:

$$\rho_c^j = \rho_c^{j-1}+\delta\rho_c\left(1-\frac{\rho_c^{j-1}}{\rho_{c_{max}}}\right). \quad (4)$$

After multiplying by $\beta$ and using Eqn (1), expression (4) takes the form

$$\Delta n_c^j = \Delta n_c^{j-1}+\delta n_c\left(1-\frac{\Delta n_c^{j-1}}{\Delta n_{c_{max}}}\right), \quad (5)$$

where $\delta n_c = \beta\delta\rho_c$, $\Delta n_c^{j-1} = \beta\rho_c^{j-1}$ and $\Delta n_{c_{max}} = \beta\rho_{c_{max}}$ are the increments of the refractive index after exposure to the first pulse and $j-1$ pulses and upon saturation under conditions of multipulse excitation, respectively.

According to experiments performed in [31], after exposure to about ten radiation pulses at $\lambda = 3100$ nm, the CC concentration is close to saturation and, accordingly, the increment $\Delta n_c^{j<10}$ is close to $\Delta n_{c_{max}}$. At saturation (5), the contribution of an individual pulse $\delta n_c(1-\Delta n_c^{j-1}\Delta n_{c_{max}}^{-1})$ to the total increment decreases with an increase in its number $j$. The change in the refractive index accumulated after the tenth pulse is close to saturated ($\Delta n_c^{j=10} \cong \Delta n_{c_{max}}$) if the increment from the first pulse is

$$\delta n_c = 0.1\Delta n_{c_{max}}. \quad (6)$$

Hence, in accordance with Eqns (1) and (3), for a given maximum increment of the refractive index $\Delta n_{c_{max}}$, the estimate for the product of the introduced parameters $\beta h$ follows:

$$\beta h = \frac{0.1\Delta n_{c_{max}}}{\delta\rho_{eh}+\delta\rho_{ex}}, \quad (7)$$

where $\delta\rho_{eh}$ and $\delta\rho_{ex}$ are the weighted average concentrations of electron–hole pairs and excitons obtained by solving equations (2a), (2b) numerically. It should be noted that the product of the parameters $\beta h$ determines the increment of the refractive index $\delta n_c$ and, accordingly, the rate at which the refractive index reaches saturation $\Delta n_{c_{max}}$ with an increase in the number of pulses. However, the numerical value of $\beta h$ does not affect the qualitative picture of the modification process.

The maximum increment of the refractive index in LiF during 'colouring' depends on the spectral range, specific colouring conditions and can reach $10^{-2}$–$10^{-4}$. In Ref. [19], the increase in the refractive index of LiF coloured by an electron beam, measured in the spectral range 600–850 nm, reached 0.05. For LiF coloured by femtosecond laser pulses, the increment of the refractive index, according to estimates made in Ref. [32], was on the order of $10^{-4}$, while, according to measurements in Ref. [33] using an induced diffraction grating, it reaches 0.01. The experimental results presented in Fig. 1 indicate the formation of a waveguide structure, an increase in its length with an increase in the number of pulses, and the existence of a LB at the exit from it with characteristic oscillations caused by induced CCs. In the case of Kerr nonlinearity, the manifestation of waveguide capture of radiation is possible if the positive increment in the refractive index of the induced structure is not less than the change caused by the nonlinearity. The latter exceeds 0.02 at a peak radiation intensity of about $3\times10^{14}$ W cm$^{-2}$, which is achieved in the case of spatiotemporal pulse compression and LB formation. In this

work, the formation of micromodification in LiF is numerically investigated at the maximum increment in the refractive index $\Delta n_{c_{max}} = 0.025$ for the saturated concentration $\rho_{c_{max}}$ of stable colour centres.

In the approximation of a slowly varying amplitude, the propagation of the $j$th pulse in the coordinate system travelling with the group velocity has the following form for AGVD:

$$2i\frac{\partial A^j}{\partial z} = \left[\frac{\Delta_\perp}{k_0} + k_2\frac{\partial^2}{\partial\tau^2} + \frac{2k_0}{n_0}(n_2 I^j + \Delta n_p^j + \Delta n_c^{j-1}) - i\frac{U}{I^j}\left(\frac{\partial\rho_e^j}{\partial\tau} + \frac{\partial\rho_{ex}^j}{\partial\tau}\right)\right]A^j. \quad (8)$$

Here $A^j(\boldsymbol{r},\tau)$ is the complex amplitude of the $j$th pulse [subscript $j$ in (8) and other expressions denotes the pulse number], represented as a function of the spatial coordinate $\boldsymbol{r}$ and 'retarded' time $\tau$, related to laboratory time $t$ by the relation $\tau = t - zn_0/c$ ($n_0 = 1.363$ is the linear refractive index, and $c$ is the speed of light in vacuum). The concentrations of free electrons $\rho_e^j$ and excitons $\rho_{ex}^j$ in (8) are functions of the coordinate $\boldsymbol{r}$ and the running time $\tau$, for which Eqns (2a) and (2b) are valid with the formal replacement of $t$ by $\tau$. Operator $\Delta_\perp$ is the transverse Laplacian; $k_0 = \omega_0 n_0/c$ is the wave number at the centre frequency $\omega_0$, corresponding to a wavelength of 3200 nm in vacuum; $n_2 = 8.1\times10^{-17}$ cm$^2$ W$^{-1}$ is the cubic nonlinearity coefficient; $k_2 = |\partial^2 k/\partial\omega^2|_{\omega=\omega_0} = 296$ fs$^2$ mm$^{-1}$ is the absolute value of the group velocity dispersion coefficient; $I^j(\boldsymbol{r},\tau) = \frac{1}{2}c_0 n_0\varepsilon_0|A^j(\boldsymbol{r},\tau)|^2$ is the intensity of the $j$th pulse; $\Delta n_c^{j-1}(\boldsymbol{r})$ is the total increment of the refractive index induced by the previous $j-1$ pulses; and $U = 12.8$ eV is the exciton absorption energy. Equation (8) describes diffraction, dispersion in the second approximation, Kerr and plasma nonlinearities for the current pulse, refraction by modifications of the refractive index, and losses

$$i\frac{U}{I^j}\left(\frac{\partial\rho_e^j}{\partial\tau} + \frac{\partial\rho_{ex}^j}{\partial\tau}\right),$$

associated with the generation of free electrons and excitons. The refractive index of the laser plasma $\Delta n_p^j(\boldsymbol{r},\tau)$ created by the $j$th pulse is determined by the concentration of free electrons $\rho_e^j(\boldsymbol{r},\tau)$:

$$\Delta n_p^j(\boldsymbol{r},\tau) = -\frac{e^2\rho_e^j(\boldsymbol{r},\tau)}{2n_0\omega_0^2 m_e\varepsilon_0}, \quad (9)$$

where $e$ and $m_e$ are the electron charge and mass, and $\varepsilon_0$ is the electrical constant. Note that excitons, unlike electrons, do not defocus radiation.

The closed system of Eqns (2)–(9) with a given space-time profile of the incident radiation describes the process of LiF modification during the accumulation of CCs induced by pulsed radiation. Solving Eqns (2) for the concentration of free electrons $\rho_e(\boldsymbol{r},\tau)$ and excitons $\rho_{ex}(\boldsymbol{r},\tau)$ in the light field, using conditions (3)–(7), which describe the accumulation of the CC concentration and the increment of the refractive index under saturation conditions, and solving the equations of nonlinear optics (8) and (9) for the field amplitude with Kerr and plasma nonlinearities, we determined the spatiotemporal variation in the pulse amplitude in LiF and the refractive index of the medium with an increase in the number of acting pulses.

Coefficient $\alpha$, which is proportional to the relative contribution of the exciton CC generation channel, is a free parameter of the model, since there are no estimates of the relative contribution of different CC generation channels in the LiF crystal. In the case of exposure to mid-IR radiation at a power slightly exceeding the critical self-focusing power, the exciton channel of CC formation without plasma generation in the filament can prevail. The plasma-free regime of CC formation was recorded in [31] using filaments in which intensity clamping occurs not because of plasma formation, but because of nonlinear losses during multiphoton absorption in the LiF exciton band. To estimate the influence of the parameter $\alpha$, we numerically calculated the increment of the refractive index after the action of one pulse $\Delta n_c^{j=1}(\boldsymbol{r})$ with the formation of colour centres only through the electron–hole channel ($\alpha = 0$), as well as only through the exciton channel ($\alpha = 1$). As a result of solving system (2)–(9) in cylindrical coordinates $\boldsymbol{r} = (r,z)$, it was found that upon plasma generation ($\alpha = 0$), after exposure to one pulse, a sequence of two spaced regions of modification is formed (Fig. 3a), which contradicts the

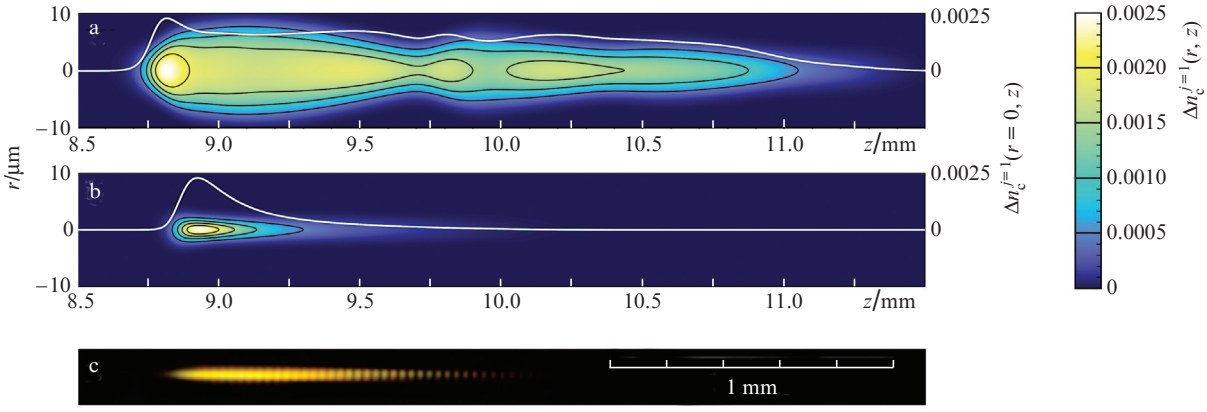


**Figure 3.** (Colour online) Colour maps of the transverse distribution of the refractive index increment $\Delta n_c^{j=1}(r,z)$ and the change in the increment on the axis $\Delta n_c^{j=1}(r=0,z)$ (white lines) along the CC structure induced in LiF after exposure to one pulse, obtained numerically based on the model of photoexcitation of the electronic subsystem (a), the model of direct creation of excitons (b), and experimentally recorded tracks of luminescent radiation after exposure to one pulse (c). The initial radius of the pulsed radiation beam at half-height of the intensity profile is 120 μm, the wavelength is 3200 nm, the pulse duration is 100 fs, and the energy is $W = 25$ μJ. The pulse travels from left to right.

results of the experiment (Fig. 3c). At $\alpha = 1$, corresponding to the presence of only a direct channel for the creation of excitons, after the action of one pulse, a distribution of the induced change in the refractive index $\Delta n_c^{j=1}(r)$ (Fig. 3b) is formed, which is close to the experimentally recorded luminescence track (Fig. 3c). In this case, the pulse spectrum calculated in the model with an exciton CC generation channel is close to that recorded in [28].

The performed analysis allows us to assume that the exciton channel dominates in the formation of a CC structure, and a model including Eqns (2)–(9) with $\Delta n_p^j(\boldsymbol{r},\tau) = 0$ and $\alpha = 1$ is applicable for the numerical study of the process of its formation.

## 4. Numerical study of the formation of a waveguide upon generation of colour centres in LiF

The process of accumulating the medium modifications was studied under the action of collimated radiation in the form of a sequence of Gaussian pulses with an axisymmetric initial intensity profile:

$$A(r,z=0,\tau) = A_0 \exp\left(-\frac{r^2}{2r_0^2} - \frac{\tau^2}{2\tau_0^2}\right), \tag{10}$$

where $A_0$ is the initial peak amplitude of the light field, and $r_0$ and $\tau_0$ are the initial beam radius and pulse duration at the $e^{-1}$ level, respectively. We consider a wave packet (10) at $\lambda =$ 3200 nm with parameters close to the experimental ones: $r_0 =$ 72 μm (corresponds to a FWHM beam diameter of 120 μm), $\tau_0 = 60$ fs (corresponds to a FWHM duration of 100 fs), and pulse energy $W = 25$ μJ. In this case, the peak power of the pulse is $P_{peak} = 230$ MW, which is $1.7P_{cr}$, where $P_{cr} = 139$ MW is the critical power of cw self-focusing in LiF. For the radiation under consideration, the wave parameters are close: $L_{diff} \sim L_{disp}$, where the diffraction length is $L_{diff} = 1.4$ cm, the dispersion length is $L_{disp} = 1.2$ cm, and under AGVD conditions, a consistent compression of the wave packet in space and time occurs [34]. In the numerical study, for each pulse, the system of Eqns (2)–(8) was sequentially solved for $\Delta n_p^j(r,z,\tau) = 0$ and $\alpha = 1$. As a result, we determined for LiF the spatial distributions of the CC concentration $\rho_c^j(r,z)$, the increments of the refractive index $\Delta n_c^j(r,z)$ accumulated after the $j$th pulse, and the distribution of the energy density (fluence)

$$F'(r,z) = \frac{c_0 n \varepsilon_0}{2} \int_{-\infty}^{\infty} |A^j(r,z,\tau)|^2 \mathrm{d}\tau$$

in pulses propagating in the induced structure.

To compare the results obtained with the experimental data, in which the total luminescence signal is recorded in the direction perpendicular to the axis of the induced structure, the integral increment of the refractive index along one of the transverse coordinates was calculated:

$$\eta^j(y,z) = \int_{-\infty}^{\infty} \Delta n_c^j(\sqrt{x^2+y^2},z)\mathrm{d}x. \tag{11}$$

The process of accumulation of the medium modification under the action of a sequence of 200 pulses is illustrated in Fig. 4, where the relative distributions $\hat{\eta}^j(y,z) = \eta^j(y,z)/w$ for $j$ from 1 to 200 are shown as colour maps. The normalisation factor $w = \max|\eta^{j=200}(y,z)|$, equal to the maximum value in the integral increment $\eta^{j=200}(y,z)$, is introduced for the convenience of comparing the values. In this case, the first pulse propagates in an unperturbed medium, and the next, starting from the second, in a structure with a modified refractive index produced by the previous pulses.

It can be seen that modification in LiF begins at a distance $z \approx 8.8$ mm, at which the radiation intensity increases during filamentation. Due to the consistent compression of the wave packet in space and time in the Kerr medium with AGVD, the distance to the starting point of filamentation is less than the distance of stationary self-focusing of the cw beam $z_{st} \approx$ 9.2 mm, estimated using the Marburger–Talanov formulae [7, 35].

With an increase in the number of pulses, the increment of the refractive index increases, starting to saturate on the axis at $j > 10$. The increase in the length of the induced modification in the direction of pulse propagation is much greater than in the opposite direction (Fig. 4). This character of the induced change in the refractive index is associated with the fact that the length of the tail part of the induced structure, in which the increment decreases, is much larger than its leading edge. Therefore, with the accumulation of modification, the increase in the length of the structure occurs mainly in its tail with an increase in the refractive index up to saturation. For a larger number of pulses ($j > 50$), the increment of the refractive index on the axis $\Delta n_c^j(r=0,z)$ changes nonmonotonically with distance (Fig. 4), which is associated with a decrease in the exciton concentration growth rate due to a significant decrease in the radiation energy caused by losses for exciton formation. In pulses with $j > 100$, the energy losses due to the formation of CCs at the beginning of propagation decrease due to saturation of the CC concentration. With further propagation, the energy density (fluence) $F'(r,z)$ on the axis increases because of Kerr self-focusing (Fig. 5), due to which the increment of the refractive index again increases up to saturation. Thus, under the conditions of pulse energy absorption during the formation of colour centres in LiF, a refocusing effect occurs, similar to that observed in a femtosecond filament upon compression of a radiation beam defocused by an induced laser plasma in the absence of absorption [6].

The accumulated modification under saturation conditions leads to a change in the profile of the structure cross section with an increase in the number $j$ of pulses. Figure 6 shows the radial distribution of the refractive index increment for various numbers of pulses, from 1 to 200, at $z = 8.9$ mm. The increment c $\Delta n_c^j$ increases most rapidly after a few first pulses (up to $j < 20$) and slows down with approaching saturation. The increment distribution over the cross section of the beam has a shape close to Gaussian until saturation is reached. As the increment grows with the number of pulses increasing to $j > 20$, its radial distribution assumes a table-like shape due to saturation. The diameter of the structure induced by 200 pulses is more than 4 μm at the $e^{-1}$ level.

The effect of colour centres on pulse propagation is illustrated in Fig. 7, where the space-time distributions of the radiation intensity $I^{j=201}(r,\tau)$ in the 201st pulse propagating in the structure induced by the previous 200 pulses are shown at two characteristic distances. The distributions are normalised to the initial peak radiation intensity $I_0$. It can be seen that in the induced structure, despite the absence of the refractive index gradient in the paraxial region, the waveguide captures radiation reflected from its boundaries (Fig. 7a). At a

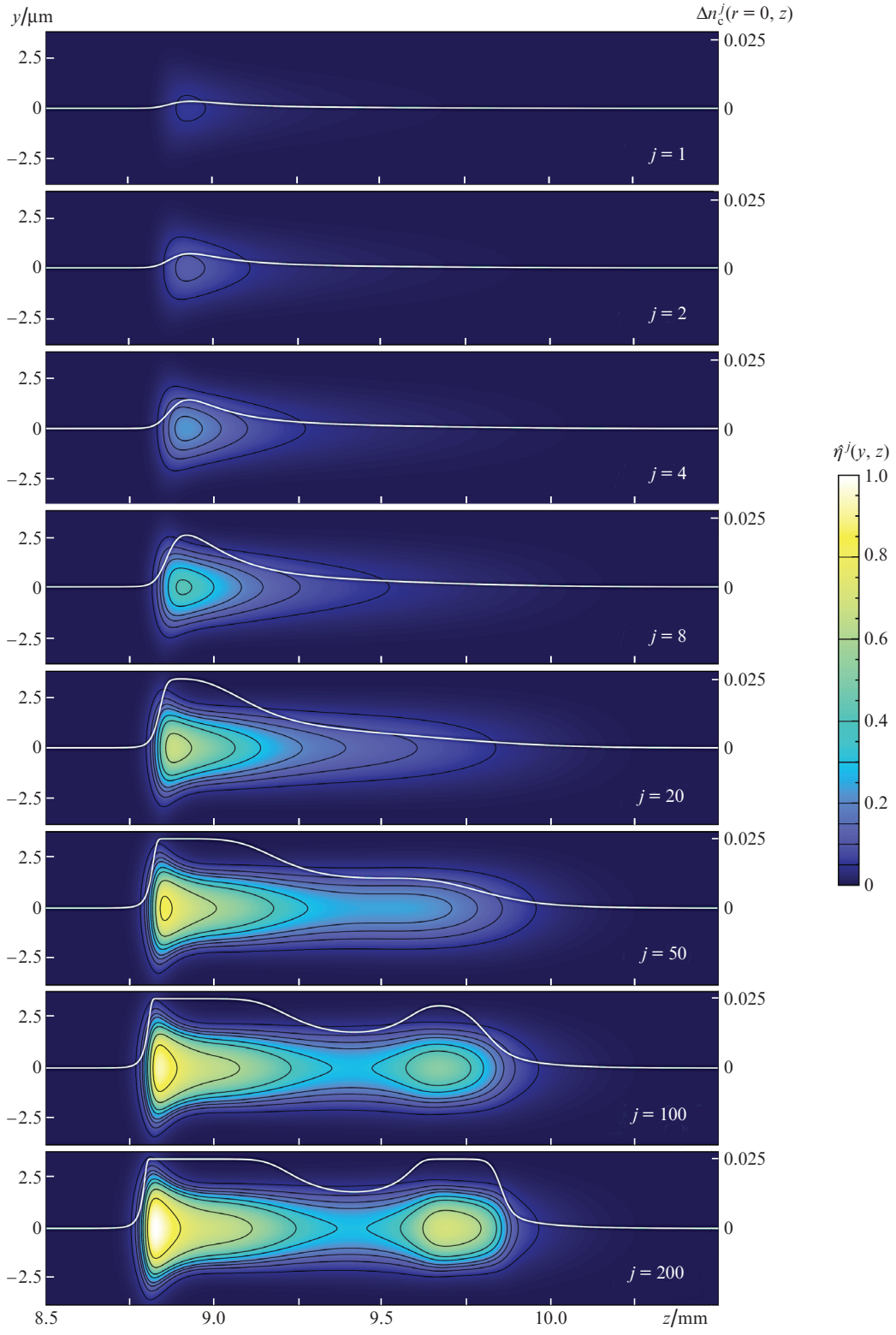


**Figure 4.** (Colour online) Colour maps of the transverse distribution of the relative increment of the refractive index $\hat{\eta}^j(y,z) = \eta^j(y,z)/\max\{\eta^{j=200}(y,z)\}$, where $\max\{\eta^{j=200}(y,z)\}$ is the maximum integrated increment $\eta^j(y,z)$ at $j = 200$. Black lines of equal level ($\hat{\eta}^j(y,z) = \text{const}$) in the $(y,z)$-plane correspond to the values 0.05, 0.1, 0.15, 0.2, 0.3, 0.4, 0.6 and 0.8. White lines show the increments of the refractive index $\Delta n_c^j(r = 0,z)$ on the axis along the CC structure induced in LiF with an increase in the number of acting pulses $j$ from 1 to 200 at $\Delta n_{c_m} = 0.025$. The initial radius of the pulsed radiation beam at half the height of the intensity profile is 120 μm, the wavelength is 3200 nm, the pulse duration is 100 fs, and the energy is $W = 25$ μJ. The pulses travel from left to right.

distance $z = 9.0$ mm, where the structure is already formed (see Fig. 4), the radiation is localised near the axis in a region with a diameter of about 8 μm. In this case, the pulse retains a symmetric shape and in its centre with the highest intensity, the spatial compression is supplemented by nonlinear compression of radiation in time due to AGVD. The aberrational

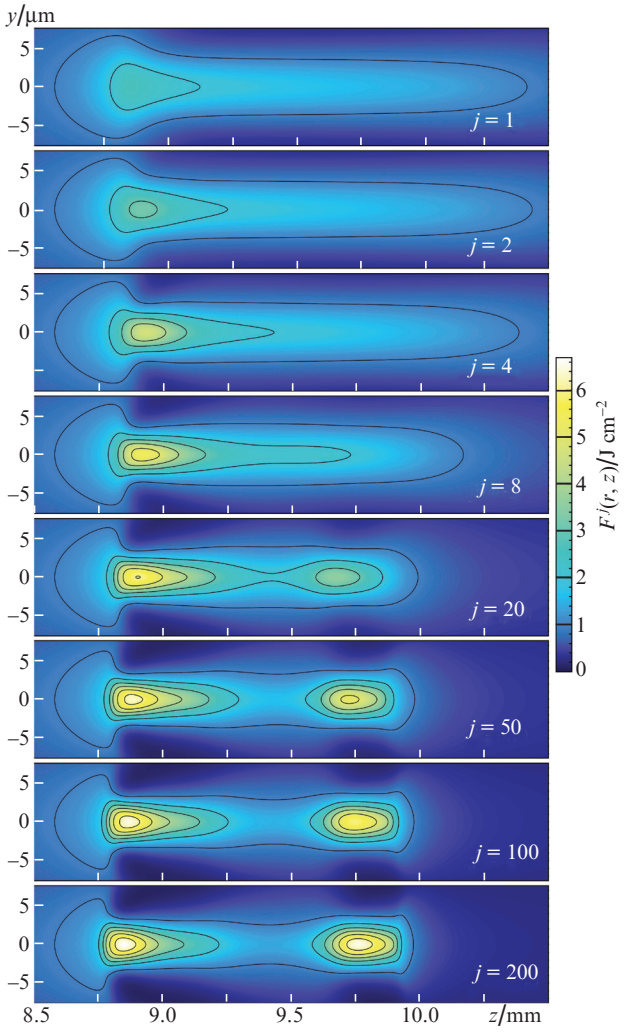


**Figure 5.** (Colour online) Fluence distribution $F^j(r,z)$ with an increase in the number of acting pulses $j$ from 1 to 200 at $\Delta n_{e_{max}} = 0.025$. Black lines of equal level $F^j(r,z) = \text{const}$ are plotted with a step of 1 J cm$^{-2}$. The initial radius of the pulsed radiation beam at half the height of the intensity profile is 120 μm, the wavelength is 3200 nm, the pulse duration is 100 fs, the energy is $W = 25$ μJ. The pulses travel from left to right.

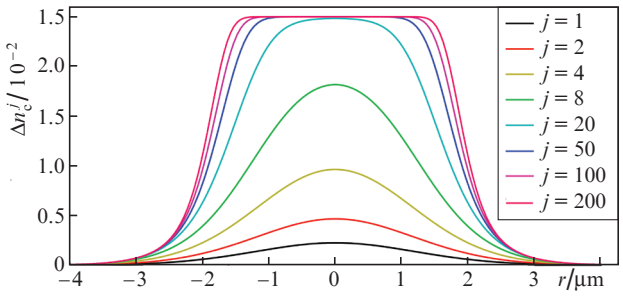


**Figure 6.** (Colour online) Lateral distribution of the refractive index increment $\Delta n_e^j(r,z)$ at $z = 8.9$ mm in a structure induced by a different number of pulses $j$ (from 1 to 200) at $\Delta n_{e_{max}} = 0.025$. The initial radius of the pulsed radiation beam at half the height of the intensity profile is 120 μm, the wavelength is 3200 nm, the pulse duration is 100 fs, and the energy is $W = 25$ μJ.

nature of the space-time compression leads to the formation of a system of interference maxima in the radiation upon reflection from the structure boundaries. This is especially

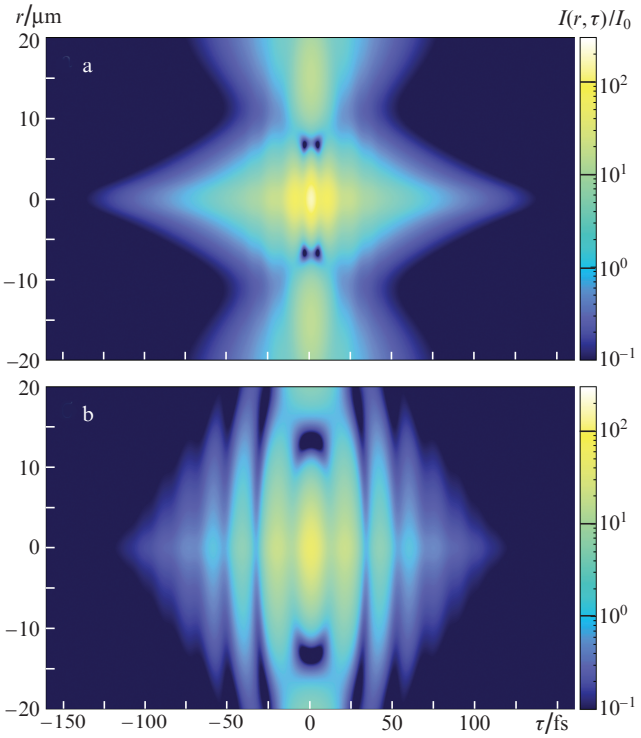


**Figure 7.** (Colour online) Spatiotemporal distribution of the relative radiation intensity $I^{j=201}(r,t)/I_0$ in the 201st pulse at distances $z =$ (a) 9.0 and (b) 9.4 mm in the structure induced by the accumulated action of 200 pulses and $\Delta n_{e_{max}} = 0.025$. The initial radius of the pulsed radiation beam at half-height of the intensity profile is 120 μm, the wavelength is 3200 nm, the pulse duration is 100 fs, and the energy is $W = 25$ μJ.

noticeable at a distance of $z = 9.4$ mm when the radiation diverges at the exit from the first part of the induced structure and the Kerr nonlinearity is weakened (Fig. 7b).

## 5. Influence of pulse energy fluctuations on waveguide formation

In experiments with exposure of LiF crystals to a series of pulses with continuous movement of the crystal in the transverse direction, it was noticed that the distance from the input surface to the created CC structures randomly changes from pulse to pulse due to fluctuations of their energy [25]. To analyse the effect of fluctuations in the pulse energy on the formation of structures, we simulated the accumulation of refractive index modification under the action of a sequence of pulses with randomly varying energy. The number of pulses in the simulated sequence was 200. The initial pulse energy was set random in accordance with the normal probability density distribution with an average value of $\bar{W} = 25$ μJ and a standard (RMS) deviation of 5%. As before, the initial radius of the pulsed radiation beam at half the height of the intensity profile was 120 μm, the pulse duration was 100 fs, and the wavelength was 3200 nm. In this case, according to estimates using the Marburger–Talanov formula, the distance from the entrance surface of the sample to the start of the filament randomly changes from the standard deviation of about 0.8 mm. The calculation result is illustrated in Fig. 8a, which shows a colour map of the distribution of the relative increment of the refractive index $\hat{\eta}^j(y,z) = \eta^j(y,z)/\max\{\eta^j(y,z)\}$ after exposure to 200 pulses ($j = 200$)

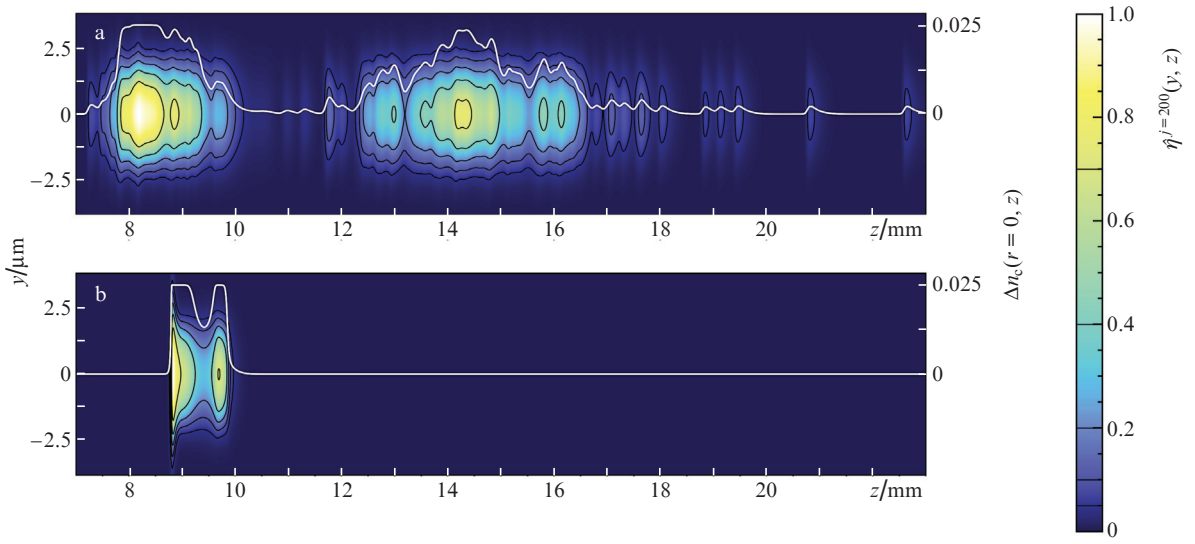


**Figure 8.** (Colour online) Colour map of the distribution of the refractive index relative increment $\hat{\eta}^j(y,z) = \eta^j(y,z)/\max\{\eta^j(y,z)\}$ for a structure induced by 200 pulses, the energy of which was a random variable with a normal distribution law at an RMSD of 5% and the average value $\bar{W}$ = 25 μJ (a), as well as the distribution pattern $\hat{\eta}^j(y,z)$ at a constant pulse energy $W$ = 25 μJ (b). Black lines of equal level $\hat{\eta}^j(y,z)$ = const correspond to 0.05, 0.1, 0.2, 0.4, and 0.7. White lines show the increments of the refractive index on the axis $\Delta n_c^j(r = 0,z)$.

with energy fluctuations. Here $\max\{\eta^j(y,z)\}$ is the maximum value of the integral increment $\eta^{j=200}(y,z)$, so that the values $\hat{\eta}^j(y,z)$ do not exceed one. For comparison, Fig. 8b shows the distribution $\hat{\eta}^j(y,z)$ on the same scale for a sequence of pulses with constant energy $W$ = 25 μJ. It can be seen that when the fluctuations of the pulse energy are taken into account (Fig. 8a), the shape of the induced channel changes qualitatively, its structure approaches that recorded in the experiment (see Fig. 1). The displacement of the beginning of the induced channel in the direction opposite to the propagation of radiation, as in the experiment, is about 1 mm (see Fig. 2). The modification along the channel changes nonmonotonically, its length significantly increases in comparison with the case without fluctuations (Fig. 8b).

## 6. Conclusions

Let us formulate the main results of the work.

1. In the regime of multipulse filamentation of femtosecond mid-IR laser radiation, an extended waveguide is formed in the LiF crystal as a result of the accumulation of the crystal modification during the generation of colour centres under conditions of saturation of their concentration. The length of the waveguide increases with an increase in the number of acting pulses both in the direction of propagation of radiation and in the opposite direction, reaching about 5 mm upon an exposure to several thousand pulses.

2. A change in the refractive index in LiF occurs upon the accumulation of colour centres under conditions of saturation of their concentration, fluctuations of the pulse energy, and waveguide capture of radiation by the structure induced by the pulses.

3. The proposed model of waveguide formation in LiF, which includes both direct exciton and electron–hole CC generation channels, describes the main processes of the refractive index change during the generation of long-lived CCs under multipulse exposure. The model of a plasma-free direct exciton production channel reproduces the modification of the refractive index with an increase in the number of pulses, which is close to that recorded experimentally in the CC luminescence tracks. Within the framework of this model, the refractive index in the waveguide under multipulse exposure changes nonmonotonically along the axis, its transverse distribution has a table-like shape with a diameter of more than 4 μm, which leads to localisation of radiation on the axis when reflected from the waveguide boundaries. Energy fluctuations in the impacting pulses lead to a significant increase in the length of the waveguide in the opposite direction due to a reduction in the average distance to its beginning and in the accompanying direction due to the refocusing effect observed during femtosecond filamentation.

***Acknowledgements.*** The experiments performed on the unique scientific facility 'Multipurpose Femtosecond Laser-Diagnostic Spectrometric Complex' at the Institute of Spectroscopy of the Russian Academy of Sciences were funded by the Russian Science Foundation (Project No. 18-12-00422). A.V.K. is grateful to Project No. 0243-2021-0004 within the framework of the Plan for Fundamental Research of the Russian Academy of Sciences for the period up to 2025 for funding part of theoretical studies (Sections 3–5).

## References

1. Davis K.M., Miura K., Sugimoto N., Hirao K. *Opt. Lett*., **21**, 1729 (1996).
2. Miura K., Qiu J., Inouye H., Mitsuyu T., Hirao K. *Appl. Phys. Lett*., **71**, 3329 (1997).
3. Nolte S., Will M., Burghoff J., Tuennermann A. *Appl. Phys. A*, **77**, 109 (2003).
4. Martinez A., Dubov M., Khrushchev I., Bennion I. *Electron. Lett*., **40**, 1170 (2004).
5. Zagorulko K.A., Kryukov P.G., Larionov Yu.V., Rybaltovsky A.A., Dianov E.M., Chekalin S.V., Matveets Yu.A., Kompanets V.O. *Opt. Express*, **12**, 5996 (2004).
6. Kandidov V.P., Shlenov S.A., Kosareva O.G. *Quantum Electron*., **39**, 205 (2009) [*Kvantovaya Elektron*., **39**, 205 (2009)].
7. Chekalin S.V., Kandidov V.P. *Phys. Usp*., **56**, 123 (2013) [*Usp. Fiz. Nauk*, **183**, 133 (2013)].

8. Yamada K., Watanabe W., Toma T., Itoh K., Nishii J. *Opt. Lett*., **26**, 19 (2001).
9. Watanabe W., Asano T., Yamada K., Itoh K., Nishii J. *Opt. Lett*., **28**, 2491 (2003).
10. Minoshima K., Kowalevicz A.M., Hartl I., Ippen E.P., Fujimoto J.G. *Opt. Lett*., **26**, 1516 (2001).
11. Chen H., Chen X., Xia Y., Liu D., Li Y., Gong Q. *Opt. Express*, **15**, 5445 (2007).
12. Szameitt A., Blömer D., Burghoff J., Pertsch T., Nolte S., Tünnermann A. *Appl. Phys. B*, **82**, 507 (2006).
13. Yamada K., Watanabe W., Nishii J., Itoh K. *J. Appl. Phys*., **93**, 1889 (2003).
14. Yamada K., Watanabe W., Li Y., Itoh K., Nishii J. *Opt. Lett*., **29**, 1846 (2004).
15. Cheng Y., Sugioka K., Midorikawa K., Masuda M., Toyoda K., Kawachi M., Shihoyama K. *Opt. Lett*., **28**, 1144 (2003).
16. Chan J.W., Huser T., Risbud S., Krol D.M. *Opt. Lett*., **26**, 1726 (2001).
17. Mao S.S., Quéré F., Guizard S., Mao X., Russo R.E., Petite G., Martin P. *Appl. Phys. A*, **79**, 1695 (2004).
18. Gaižauskas E., Mizeikisb V., Misawa H., Kudryashov S.I., Zvorykin V.D., Ionin A.A., Juodkazis S. *Proc. SPIE*, **7214**, 72140S-1 (2009).
19. Baldacchini G. *J. Lumin*., **100**, 333 (2002).
20. Klinger M.I., Lushchik Ch.B., Mashovets T.V., Holodar G.A., Sheinkman M.K., Elango M.A. *Sov. Phys. Usp*., **28**, 994 (1985) [*Usp. Fiz. Nauk*, **147**, 523 (1985)].
21. Lushchik A., Kirm M., Lushchik Ch., Vasil'chenko E. *Nucl. Instrum. Meth. B*, **166-167**, 529 (2000).
22. Martynovich E.F., Dresvyansky V.P., Rakevich A.L., Lazareva N.L., Arsentieva M.A., Tyutrin A.A., Bukhtsoozh O., Enkhbat S., Kostryukov P.V., Perminov B.E., Konyashchenko A.V. *Appl. Phys. Lett*., **114**, 121901 (2019).
23. Martynovich E.F., Glazunov D.S., Grigorova A.A., Starchenko A.A., Kirpichnikov A.V., Trunov V.I., Merzlyakov M.A., Petrov V.V., Pestryakov E.V. *Opt. Spectrosc*., **105**, 348 (2008) [*Opt. Spektrosk*., **105**, 380 (2008)].
24. Martynovich E.F., Kuznetsov A.V., Kirpichnikov A.V., Pestryakov E.V., Bagaev S.N. *Quantum Electron*., **43**, 463 (2013) [*Kvantovaya Elektron*., **43**, 463 (2013)].
25. Kuznetsov A.V., Kompanets V.O., Dormidonov A.E., Chekalin S.V., Shlenov S.A., Kandidov V.P. *Quantum Electron*., **46**, 379 (2016) [*Kvantovaya Elektron*., **46**, 379 (2016)].
26. Chekalin S.V., Kompanets V.O., Kuznetsov A.V., Dormidonov A.E., Kandidov V.P. *Laser Phys. Lett*., **13**, 065401 (2016).
27. Chekalin S.V., Kompanets V.O., Dormidonov A.E., Kandidov V.P. *Phys. Usp*., **62**, 282 (2019) [*Usp. Fiz. Nauk*, **189**, 299 (2019)].
28. Chekalin S.V., Kompanets V.O., Dormidonov A.E., Kandidov V.P. *Quantum Electron*., **47**, 259 (2017) [*Kvantovaya Elektron*., **47**, 259 (2017)].
29. Keldysh L.V. *Sov. Phys. J. Exp. Theor. Phys*., **20**, 1307 (1965) [*Zh. Eksp. Teor. Fiz*., **47**, 1945 (1965)].
30. Rohlfing M., Louie S.G. *Phys. Rev. Lett*., **81**, 2312 (1998).
31. Chekalin S.V., Kompanets V.O. *Opt. Spectrosc*., **127**, 88 (2019) [*Opt. Spektrosk*., **127**, 94 (2019)].
32. Chiamenti I., Bonfigli F., Montereali R., Kalinowski H. *J. Microw. Optoelectron. Electromagn. Appl*., **13**, 47 (2014).
33. Kurobori T., Kawamura K., Hirano M., Hosono H. *J. Phys.: Condens. Matter.*, **15**, L399 (2003).
34. Zaloznaya E.D., Kompanets V.O., Dormidonov A.E., Chekalin S.V., Kandidov V.P. *Quantum Electron*., **48**, 366 (2018) [*Kvantovaya Elektron*., **48**, 366 (2018)].
35. Goldberg V.N., Talanov V.I., Erm R.E. *Radiophys. Quantum Electron*., **10**, 368 (1967).